Assessing the Effects of Atmospheric Stability on the Inertial Subrange of Surface Layer Turbulence using Local and Global Multiscale Approaches

Bin Shi, Brani Vidakovic

School of Industrial and Systems Engineering

Georgia Institute of Technology, Atlanta, GA 30332-0205, USA

(e-mail:{bshi|brani}@isye.gatech.edu)

Gabriel G. Katul

Nicholas School of the Environment and Earth Sciences,Box 90328

Duke University, Durham, NC27708-0328, USA.

(e-mail:gaby@duke.edu)

John D. Albertson

Department of Civil and Environmental Engineering,

Duke University, Durham, NC 27708-0328, USA

(e-mail: john.albertson@duke.edu)

June 19, 2004

Abstract

The conceptual framework for modelling the inertial subrange is strongly influenced by the Richardson cascade, now the subject of various reinterpretations. One apparent departure from the Richardson cascade is attributed to boundary conditions influencing large-scale motion, which in turn, can directly interact with smaller scales thereby destroying the universal statistical scaling attributes of the inertial subrange. Investigating whether boundary conditions and inertial subrange eddies interact continues to be an active research problem in contemporary turbulence research. Using longitudinal (u), lateral (v), and vertical (w) velocities co-located with temperature (T) time series measurements collected in the atmospheric surface layer (ASL), we evaluate whether the inertial subrange is influenced by different stability regimes. The different stability regimes are proxies for different boundary conditions, as upper boundary condition force the mechanical shear and lower boundary condition force surface heating and buoyancy. The novelty of the present work lies in its combined use of global and local scaling properties (e.g. quasi-Hurst exponent, distributional properties of the wavelet coefficients, and Tsallis's thermostatic entropy measures) to assess whether atmospheric stability impacts both local and global inertial subrange scaling.

1 Introduction

The structure of turbulence in the inertial subrange has received much research attention over the past 50 years [1]. This strong interest is attributed to the possible emergence of universal or quasi-universal theories of turbulence [2, 3, 4, 5], which is a research area of interest in many fields (including finance). The inertial subrange encompasses eddies much larger than the viscous dissipation scales yet much smaller than the integral length scale (L_I) of the flow. The basic premise for the emergence of universal scaling is that large-scale anisotropic forcing characteristics (i.e. boundary effect conditions) are lost during the Richardson cascade process, thereby achieving local isotropy and universality at sufficiently smaller inertial scales [6]. However, several experiments and simulations over the past 2 decades suggest persistent effects of large scale anisotropies at these so-called inertial scales, even for very high Reynolds numbers and after many cascading steps [7]. The departure from the so-called Kolmogorov [8] view of universal scaling and subsequent refinements [9] is now supported by numerous observations and theoretical arguments regarding the anomalous scaling in measured structure functions, particularly for passive scalars [10, 3, 11, 7, 12], and static pressure [13]. The anomalous scaling is commonly attributed to short-circuiting of the energy cascade process due to the existence of organized large-scale features such as ramp-like structures, which are influenced by boundary conditions, and themselves directly influence small scale turbulence [7, 14].

To quantify whether boundary conditions influence the statistical properties of the inertial subrange for the atmospheric surface layer (ASL), we utilize two methods: (i) a global scaling self-similarity index, and (ii) a scale-wise evolution of non-parametric estimates of probability densities in the wavelet domain. Each of these measures will be applied to turbulence time series measurements collected for three atmospheric stability regimes: unstable, near-neutral, and stable stratification. An ANOVA-type technique will then be applied to asses the significance of atmospheric stability factors on these two multiscale measures. The main novelty of this work is in utilizing both global and

local multiscale measures to assess the effects of atmospheric stability on the statistical structure of the inertial subrange of several flow variables. However, before we describe these multiscale methods, a brief description of the experiment and the data set will be provided.

2 Data

Time series measurements of longitudinal (u), lateral (v), and vertical (w) velocities and air temperature (T) were collected over a grass-covered forest clearing at Duke Forest near Durham, North Carolina. The measurements were collected on June, 12-16, 1995 at 5.2 m above the grass surface using a GILL triaxial sonic anemometer. Sonic anemometers measure velocity by sensing the effect of wind on transit times of sound pulses travelling in opposite directions across a known instrument distance d_{sl} = (0.149 m in this study). The measurements were sampled at $f_s = 56Hz$ and were subsequently divided into 19.5 minute intervals to produce $N = 65,536$ time measurement per flow variable per run. Our choice of 19.5 minute intervals is a compromise between the need for stationary conditions at large scales and maximizing the statistical sample size within a given run. The experiment resulted in an ensemble of 95 runs over a wide range of atmospheric stability conditions ranging from near convective to stable atmospheric flows. Using the atmospheric surface layer stability parameter, $\xi(= z/L)$, these 95 runs were then classified in one of the three stability classes: stable, near neutral, and unstable. Here, L is the Obukhov length and z is the height from the ground surface. With this classification, 6 runs were collected in stable stability conditions, 23 runs were collected under near-neutral atmospheric stability conditions, and the rest were collected under unstable atmospheric stability conditions. We then selected 6 runs from the near neutral class and 6 runs from the unstable stability class such that the ensemble mean wind speed ($\overline{U}$) of these 6 runs were comparable to those 6 runs collected under stable atmospheric stability conditions. The scale-wise analysis utilizes these 18 runs while the global analysis makes use of all 95 runs. The ensemble mean and

standard deviation of the 6 runs for unstable, stable, and neutral wind speed are provided in Table 1. Further details about the experimental setup, atmospheric stability conditions, the various measures used in the inertial subrange identification, and instrumentation details can be found elsewhere [15, 16].

Table 1: Mean and standard deviation of the 6 runs for unstable, stable, and neutral wind speed

	Unstable	Neutral	Stable
Mean($\overline{U}$)	1.8096	1.9782	1.814
Std.($\overline{U}$)	0.0789	0.2502	0.4678

3 Methods of Analysis

In this section, the methodologies for quantifying the effects of ξ on the local and global properties of the inertial subrange are described. These methods include: (i) zero-crossing analysis resulting in a quasi-Hurst exponent, (ii) scale-wise fitting of exponential power distributions, $\mathcal{EPD}$, in the wavelet domain (and given its possible theoretical connection to the well-known Tsallis entropy measure). These analytic tools will be utilized to assess whether ξ affects the inertial subrange. We note that these measures are sensitive to different assumptions; hence, if ξ significantly affects the inertial subrange, it is likely to be resolved by these two methods.

3.1 Quasi-Hurst Exponent

The Hurst exponent (after British hydrologist H. E. Hurst, [17]) is a measure of "roughness" of self-affine time series. There are many methods to estimate the Hurst exponent of a stationary process. The zero-crossing method [18] is based on counting the number of zero crossings Z_N, producing an estimate of the Hurst exponent given by:

$$\hat{H} = \frac{1}{2}\{1 + \log_2(1 \pm |\cos(\pi S_N)|)\}, \tag{1}$$

where $S_N = Z_N/(N-1)$ is an average number of zero-crossings for the differenced time series of length N, and sign + (alternativelly –) in $\pm$ is taken if the true exponent H is above (below) 1/2. Usually, it is not difficult to decide whether the true exponent H is above or below 1/2 by observing the time series, unless the true H is close to 1/2. It was also demonstrated ([18]) that the $\hat{H}$ is asymptotically Gaussian for the fractional Brownian motion (fBm) process when the true Hurst exponent does not exceed 3/4.

The estimation of $\hat{H}$ via (1) is valid only for time series with stationary increments. For time series lacking stationary increments, such as the case in turbulence time series measurements, we call $\hat{H}$ the *quasi-Hurst* exponent. One of the attributes distinguishing turbulence signals from fBm is the distinction between the quasi-Hurst and Hurst exponents. Theoretically, the quasi-Hurst and Hurst exponents coincide for fBm since fBm has stationary increments. We empirically confirm this convergence using 1000 fBm paths constructed with a true hurst exponent of 1/3. The resulting average $\hat{H}$ is 0.3331 with standard deviation of 0.06. The p-value of a t-test for the equality of $\hat{H}$ to 1/3 is 0.9. Such a large p-value suggests that the $\hat{H}$ is an adequate estimator of the Hurst exponent for an fBm process. On the other hand, the quasi-Hurst exponent for turbulence time series measurement is quite variable and significantly exceeds 1/3. This discrepancy may be utilized to diagnose how atmospheric stability alters the global scaling parameter. That is, by analyzing deviations of $\hat{H}$ from 1/3 (or the Kolmogorov scaling) for turbulence measured under different stability conditions, a logical basis for tracking how atmospheric stability conditions impact global scaling of inertial subrange turbulence can be developed.

3.2 Evolutionary Models of Scale-Wise Empirical Densities of Wavelet Coefficients

Another method for assessing the effects of atmospheric stability on the inertial subrange is the sensitivity of the probability density function (pdf) of the wavelet coefficients of a given flow variable to variations in atmospheric stability conditions. It is a case-verified fact that

scale-wise distribution of wavelet coefficients appear similar for a variety of signals and images. Typically, such empirical distributions are symmetric with a sharp peak at zero. Guided by this opulent evidence, [19] proposed modeling a "typical" wavelet coefficient X by an exponential power family of distributions, $\mathcal{EPD}(\alpha, \beta)$, having the following pdf:

$$f(x) = Ke^{-(|x|/\alpha)^{\beta}}, \tag{2}$$

where α is the scale parameter, β is the shape parameter, and K is a normalizing constant given by $K = \beta/(2\alpha\Gamma(1/\beta))$. In the context of wavelet modeling, this approach is often referred to as Mallat's model and reduces to Gaussian for $\beta = 2$, to double exponential for $\beta = 1$ and trivially to uniform for $\beta = 0$. Hence, by investigating how ξ affects α and β at various scales, we can assess whether atmospheric stability impacts the scale-wise wavelet coefficients. Such coefficients, belonging to single scale, can be thought of as independent due to the de-correlation property of discrete wavelet transformations (DWT). To estimate these pdf parameters in $\mathcal{EPD}(\alpha, \beta)$, a moment-matching method is adopted. The method is based on matching the theoretical moments, given by

$$E(|X|) = 2K\frac{\alpha^2\Gamma(\frac{2}{\beta})}{\beta} \quad \text{and} \quad E(X^2) = 2K\frac{\alpha^3\Gamma(\frac{3}{\beta})}{\beta}, \tag{3}$$

with their empirical counterparts: $\frac{1}{N}\sum|x_i|$ and $\frac{1}{N}\sum x_i^2$. Computation of these estimators is not difficult and involves solving one non-linear equation, and the empirical counterparts for two quantities in (3) can be readily obtained. Next we explore close relationship between Mallat's model and the Tsallis Maxent distribution, now receiving broad attention in turbulence research (e.g. [20]).

3.3 Tsallis Maxent Entropy Models

The traditional entropy theory is based on Shannon's definition; more general measures, such as Renyi and Tsallis (sometimes called Tsallis-Havrda-Charvat (THC), or Havrda-Charvat entropy, since the definition of this entropy measure first was given in [21]) have also been proposed. Practical applications and theoretical implications of Tsallis-type entropy are active research areas in the physical sciences, especially turbulence [22, 20, 23, 24, 25, 26]. For example, *Tsallis thermostatistic* is based on Tsallis entropy which is a generalization of the Shannon (Boltzmann-Gibbs) entropy. The Tsallis entropy [28, 29] is given by

$$S_q = \frac{1}{q-1}\left(1 - \int_{-\infty}^{\infty} p(x)^q dx\right), \tag{4}$$

where $p(x)$ is the probability density of the microstate x of the system (in our case, the microstate refers to the individual velocity of the turbulence) and q is the non-extensive parameter (also regarded as a measure of the information incompleteness). The ordinary Shannon entropy is obtained as a special case when $q \to 1$. Tsallis' measure of entropy is more flexible than Shannon's due to its adaptive parametrization. We find that the maxent (maximum-entropy) probability distribution of a random variable X representing the turbulent measurements is constrained as follows:

$$\int_{-\infty}^{\infty} p(x)dx = 1, \text{ and} \tag{5}$$

$$\int_{-\infty}^{\infty} p(x)\epsilon_x dx = E, \tag{6}$$

where E is the energy content of x and should be a known constant, and ϵ_x's denote the energies at various microstates. The exact definition of ϵ_x in reality depends on the condition of the flow; roughly it can be taken as $\epsilon_x = x^2/2$ (x is assumed to be the velocity at this microstate). The general maximizing solution (Maxent distribution) has

the following form [30]:

$$p(x) = \frac{1}{K_q} \left(1 + (q-1)\beta_1 \epsilon_x)\right)^{\frac{1}{1-q}}, \tag{7}$$

where

$$K_q = \int_{-\infty}^{\infty} \left(1 + (q-1)\beta_1 \epsilon_x\right)^{\frac{1}{1-q}} dx \tag{8}$$

is the so-called partition function and $\beta_1 = 2/(5-3q)$ is a suitable inverse *temperature-like* variable. Interestingly, the value of q can be related to the properties of the Maxent distribution as follows.

If $1 < q < 3$, we could evaluate (8) with $\epsilon_x = x^2/2$ as

$$\begin{aligned} K_q &= \int_{-\infty}^{\infty} \left(1 + \frac{1}{2}(q-1)\beta_1 x^2\right)^{\frac{1}{1-q}} dx \\ &= \left[\frac{\pi}{\beta_1(q-1)}\right]^{0.5} \frac{\Gamma(1/(q-1) - 1/2)}{\Gamma(1/(q-1))}, \end{aligned} \tag{9}$$

where $\Gamma(\cdot)$ represents the standard Gamma function. Furthermore, the second moment is calculated when $1 < q < 5/3$ as

$$EX^2 = \frac{2}{\beta_1(5-3q)}. \tag{10}$$

However, this second moment tends to infinity if $q \geq 5/3$ and the so-called heavy-tailed distribution, which is universally recognized as a basic characteristic of turbulence, is recovered in this case.

If $q > 3$, the integral defining K_q would diverge and hence the probability density function does not exist.

If $q \to 1$, the distribution in (7) converges to normal.

If $q < 1$, the distribution in (7) would resemble a cut-off distribution. Below, we briefly explore further links between Mallat's model and the Tsallis Maxent model.

3.4 The Link between Mallat and Tsallis Maxent Models

Comparison of canonical forms of Mallat's and Tsallis models indicate close relationship between the $\mathcal{EPD}$ family and the Maxent distribution. Both of them include the uniform, normal, and Laplace distributions as special cases, as well as an infinite number of distributions with arbitrary variances and kurtosis. We demonstrate this link empirically using turbulent velocity time series. First, the turbulence time series is decomposed into three successive finest scales using discrete wavelet transformation. These scales are within the inertial subrange as discussed in [27]. We utilize the Daubechies 4-tap filter to ensure a balance of localization in time and frequency domains (i.e. a compromise between the Haar and Fourier bases). Next, we estimate the non-extensive parameter q for each scale using the relationship between q and the moments,

$$EX^m = \frac{1}{2^m} \prod_{j=0}^{m-1} \frac{5+2j}{4+j-(3+j)q}, \tag{11}$$

where X is a Maxent distributed random variable. To give an estimator of q, we utilize the kurtosis κ, which is usually defined as:

$$\kappa = \frac{EX^4}{(EX^2)^2}. \tag{12}$$

We substitute the expressions for EX^4 and EX^2 evaluated by (11) and solve (12) with respect to q. The solution is:

$$q = \frac{7\kappa - 15}{5\kappa - 9}. \tag{13}$$

Once the parameter q is evaluated, the complete form of the normalized Tsallis Maxent distribution of unit variance, which is assumed to be the theoretical distribution of wavelet coefficients, is specified. The empirical pdf's of the scale-wise wavelet coefficients are compared with the corresponding Tsallis Maxent distribution in Figure 1. In addition, we also fit Mallat's model for the scales-wise coefficients. For simplicity, the variances of these

scales-wise coefficients have been normalized to unity.

The results shown in Figure 1 suggest an almost perfect match among these three types of pdf's, especially at the tails. The large departures from the measured pdf around the center points is attributed to the "zoom effect" of logarithmic representation. The turbulence data we analyzed in Figure 1 is for a longitudinal velocity run collected in stable atmospheric conditions. The pdf's of wavelet coefficients for the other flow variables v, w and T and at different stability regimes behave similarly as those in Figure 1. We conclude that the marginal distribution of the turbulence wavelet coefficients at a fixed scale well match the maximum Tsallis entropy distribution. At the same time, the $\mathcal{EPD}$-model also fits well the empirical pdf. This empirical closeness demonstrates the inherent link between the $\mathcal{EPD}$ and the Tsallis Maxent distribution. Theoretical discussion of this link is expanded on in the Appendix.

3.5 Fitting the fBm into Mallat's Model

In contrast to turbulence data, the scale-wise densities of normalized wavelet coefficients for the fBm are invariant with respect to the scale index. This argument is supported by an ANOVA analysis based on the simulation described next. First, we generated 100 independent runs of fBm using the Wood-Chan algorithm and computed their wavelet coefficients. Second, we normalized the coefficients at each scale to have a unit variance and fit Mallat's model to these normalized coefficients. At each scale we obtained 100 shape parameters. Finally, we performed the nonparametric ANOVA analysis (Kruskal-Wallis test) to assess whether the scale affects the shape parameters. The high p-value (0.7180) indicates that shape parameters are invariant to scale.

For reference, we show the fitted $\mathcal{EPD}$ of the scale-wise wavelet coefficients for the fBm in Figure 2. Unlike turbulence, these pdf's are nearly Gaussian at all levels (scales), as theoretically expected.

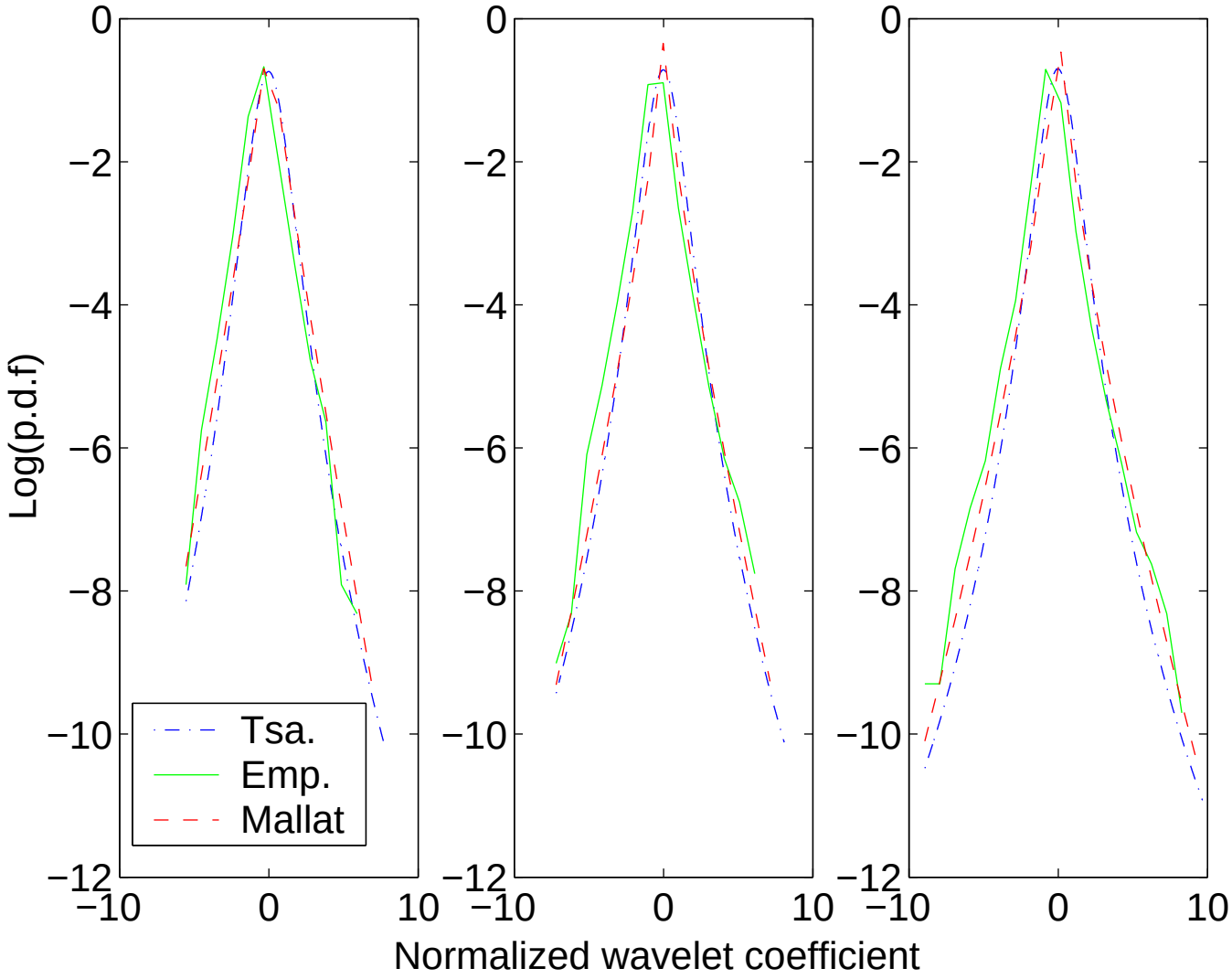

Figure 1: The comparison between Tsallis Maxent distribution (dash dot), the empirical distribution (dash), and Mallat's model (solid) at the three finest scales of the discrete wavelet transformation. The left panel is the coarsest scale, while the finest scale is at the right panel. The fitted parameters for the three scales are $q = 1.3263, 1.3575, 1.3688$, $\beta = 0.8133, 0.6467, 0.5767$ respectively from the left to the right.

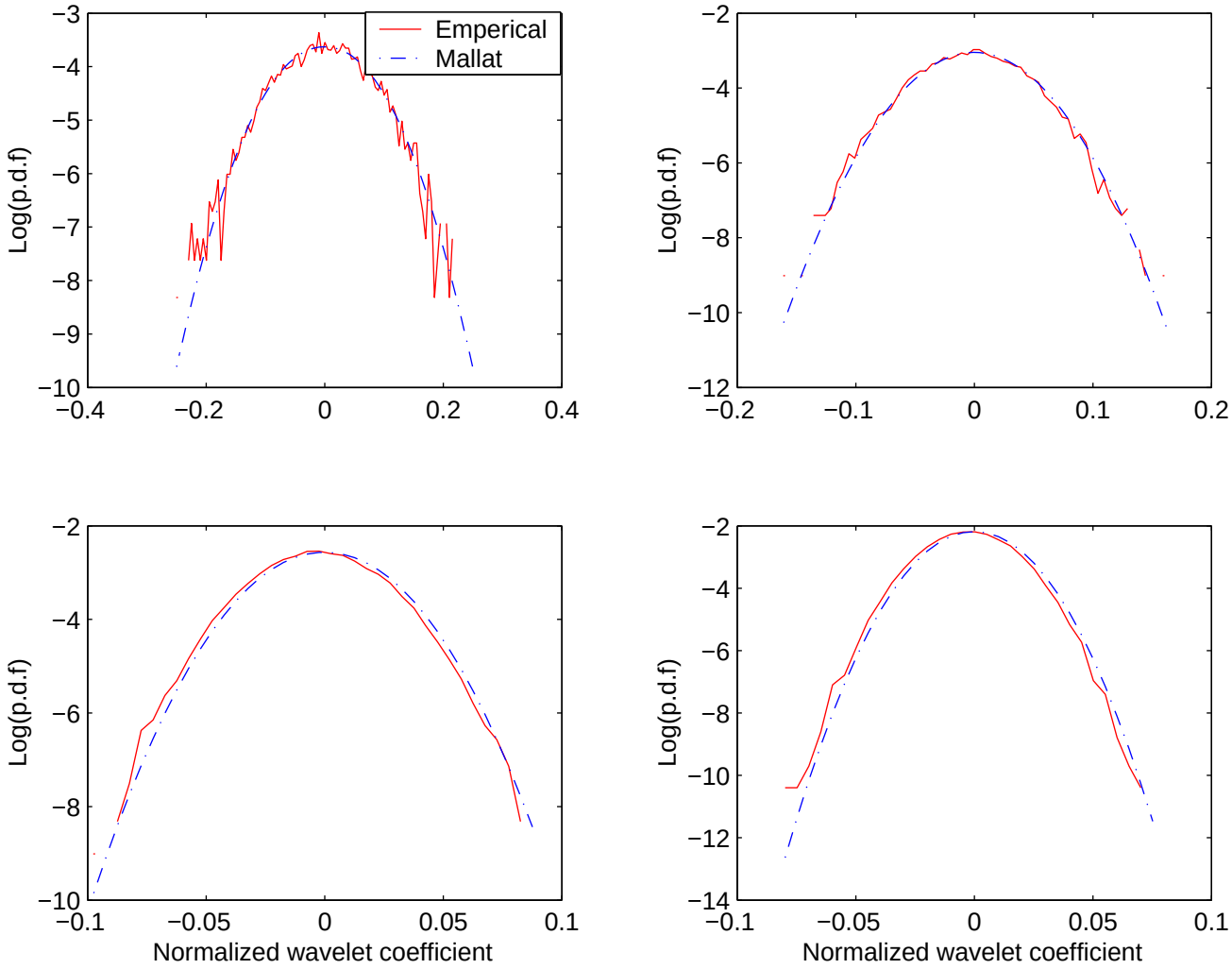

Figure 2: The logarithms of the empirical density and Mallat's model at different scales for a typical fBm having a Hurst exponent of 1/3. Four panels show the pdf analysis at the four finest scales in DWT. The top-left panel is the coarsest scale while the bottom-right panel is the finest scale. The β's at different scales are estimated from the data and are $1.7891, 1.9388, 1.9307$ and 1.9242 respectively. Note that these pdf's are approximately normal.

Table 2: Mean and standard deviation of the quasi-Hurst exponent $\hat{H}$'s for the four flow variables. The numbers in the brackets are statistics for the selected six runs for each stability regime described in the experimental setup and are reported here for reference.

Turbulence		Temperature		u		v		w	
$\hat{H}$		mean	std.	mean	std.	mean	std.	mean	std.
s	unstable	0.353	0.102	0.444	0.046	0.451	0.035	0.398	0.047
t		(0.417)	(0.043)	(0.446)	(0.026)	(0.404)	(0.045)	(0.328)	(0.032)
a	neutral	0.336	0.116	0.408	0.049	0.441	0.052	0.409	0.054
b		(0.428)	(0.049)	(0.439)	(0.035)	(0.403)	(0.066)	(0.291)	(0.105)
i	stable	0.359	0.060	0.317	0.0715	0.340	0.057	0.419	0.029
l		(0.342)	(0.056)	(0.397)	(0.052)	(0.431)	(0.054)	(0.428)	(0.041)
i	All	0.349	0.103	0.427	0.058	0.441	0.049	0.402	0.048
t		(0.323)	(0.067)	(0.412)	(0.047)	(0.438)	(0.039)	(0.413)	(0.049)

4 Atmospheric Stability Effects on the Inertial Subrange

In this section, we discuss the effects of atmospheric stability on the quasi-Hurst exponent (global scaling) and the parameters of the $\mathcal{EPD}$ distribution (local scaling). As mentioned before, the quasi-Hurst exponent ($\hat{H}$) is a global fractal index of a time series. Systematic variability of global scaling property with respect to stability factors can be used as indicator of interactions between boundary conditions and inertial subrange scaling.

For each stability class, a descriptive summary of the quasi-Hurst exponent of the four turbulent flow variables is reported in Table 2. These exponents are all calculated by the zero-crossing method.

We tested the significance of ANOVA components for the above quasi-Hurst exponents to quantify how the atmospheric stability condition affects the global fractal geometry. The results are summarized by the p-values, which are used again to test the equality of the quasi-Hurst exponents under three different stability conditions.

It is clear from these two tables that the stability impacts the longitudinal and lateral velocities most given that their respective p-values are relatively small (0.00004 and 0.003).

Hence, we conclude that ξ has a statistically discernable effect on the inertial subrange of u and v. However, ξ had no significant impact on the global fractality measures of w and T given that the corresponding p-values are large (0.43 and 0.87 respectively).

It is for this reason that we explore the scale-wise structure of turbulence in the wavelet domain. We utilize Mallat's $\mathcal{E}PD$ model to assert the findings of the global scaling analysis. The first step is to determine the pdf parameters of the normalized wavelet coefficients in the $\mathcal{E}PD$ model at each scale. After estimating the parameters for each flow variable, we can assess the significance of atmospheric stability conditions at specific scales. In this analysis, we restrict the scale-wise calculations to the finest 3 (out of 16) detail levels to insure that these wavelet coefficients fall within the inertial subrange (identified as in [31, 27]) and minimize distortions due to Taylor's hypothesis.

While the results presented in Figure 1 qualitatively demonstrate good agreement between the estimated pdf from the $\mathcal{E}PD$ family and the measured pdf, further assessed whether the parametric model is adequate via Q-Q plots presented in Figure 3. In these 3 panels, the Q-Q plots are almost straight lines with relatively few outliers at the tails. Statistically, this figure indicates good agreement between the data and the parametric model. Figure 1 and Figure 3 are actually selected from a large number of runs for the 4 flow variables and the results of other runs (not shown) support this analysis.

Again, both the pdf plots and the Q-Q plots show that $\mathcal{E}PD$ model fits well the turbulence measurements. Thus, it is natural to regard the scale-wise parameters of this model as local scale indices of turbulence. We estimated these parameters for each of the runs within each stability class and tested their equality across different atmospheric stability classes. The results from this analysis should be taken with caution because the parameter comparisons across stability regimes for a specified scale index (j) assume that the eddy sizes represented by j are the same irrespective of stability (here - the larger the j the smaller the turbulent scale). While every effort was made to select the 6 runs across different stability classes with comparable mean wind speeds, the distortions due to Tay-

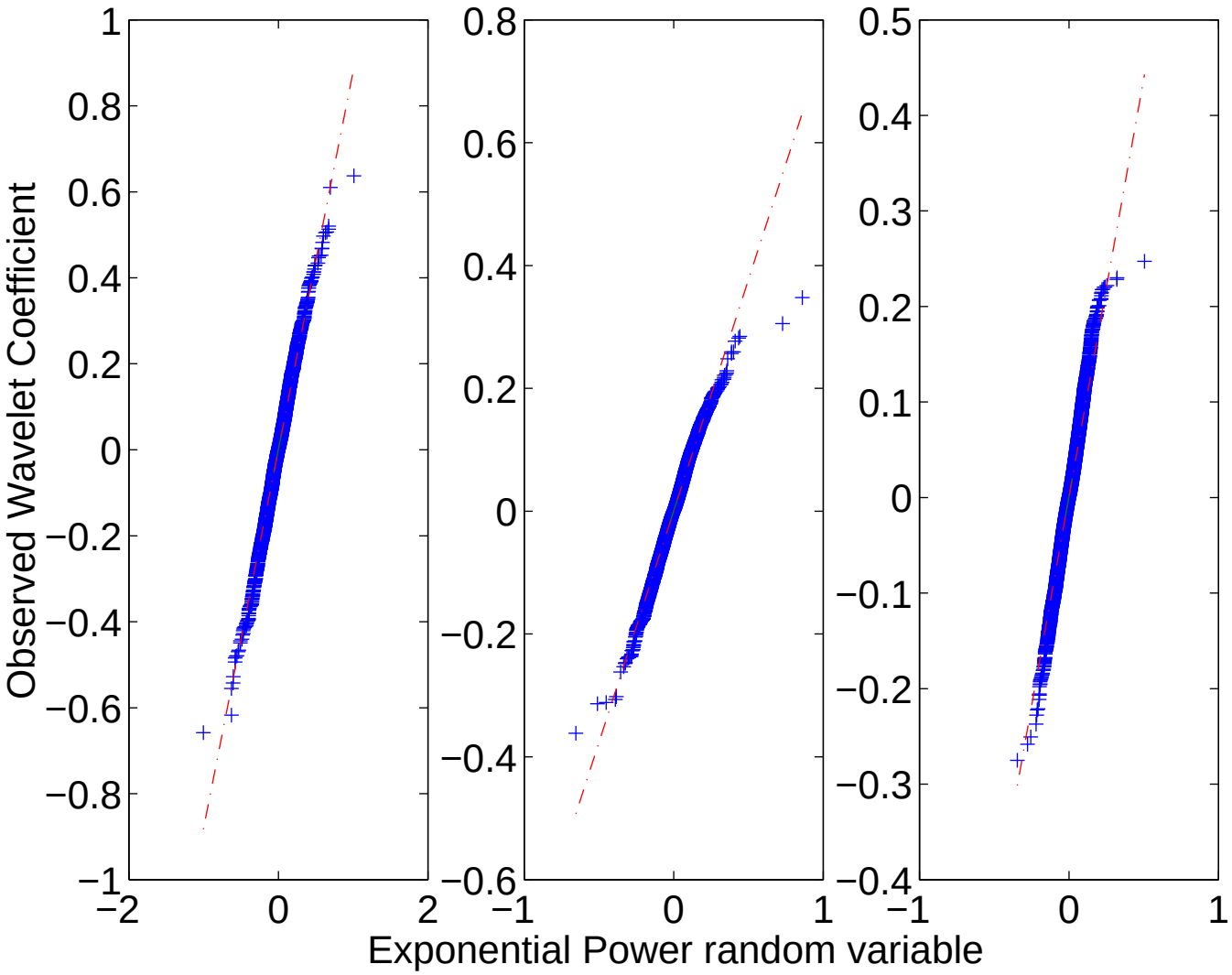

Figure 3: The Q-Q plots of the measured and modeled random variables at different scales in the wavelet domain for a typical flow variable u. The left panel shows the coarsest scale while the right panel shows the finest scale. The same turbulence measurement time series are used as in Figure 1

lor's hypothesis may dependent on atmospheric stability itself. That is, a scale index of $j = 15$ may not precisely reflect identical eddy sizes for unstable, near neutral, and stable atmospheric stability because of differences in the turbulent intensities (despite equality in mean wind speed). What makes this analysis robust to such a limitation is that the use of orthonormal wavelet transforms means that the scale $j = 15$ is not precisely mapped onto one unique frequency or wavenumber (as is the case with Fourier spectra) but a distribution of frequencies (or wavenumbers) set by the Daubechies wavelet. Hence, as long as the relative distortions attributed to the use of Taylors hypothesis across different stability classes (for the same mean wind) are much smaller than ln(2), the scale index j does represent the mean eddy sizes across different atmospheric stability regimes. Furthermore, we are restricting this local scale-wise analysis to the three finest scales known to be least affected by distortions due to finite turbulent intensity.

For each of the 6 runs in each stability class, we fitted the Mallat model for j=14,15, and 16 (out of 16) and all four flow variables. Table 3 gives the mean and standard errors of the shape parameters for each flow variable and stability class. Unlike the global analysis, we are not able to provide the ANOVA p-values since we only have six runs for each regime. This small number of runs makes the statistical inference difficult. As a remedy procedure, we provide the Box plots for these shape coefficients to compare the difference across the stability regimes in Figure 4. Figure 4 demonstrates that β for all the flow variables, stability regimes, and inertial scales is far from Gaussian ($\beta = 2$), and is closer to a double exponential ($\beta = 1$). The lowest β (i.e. most heavy-tailed) is for temperature at the finest level (irrespective of stability regime). Furthermore, the fastest change in β with scale (i.e. a measure of increased intermittency with decreasing scale) is also for the temperature irrespective of stability class. Hence, the local analysis here clearly demonstrates scale-wise dissimilarity between temperature and velocity within the inertial subrange.

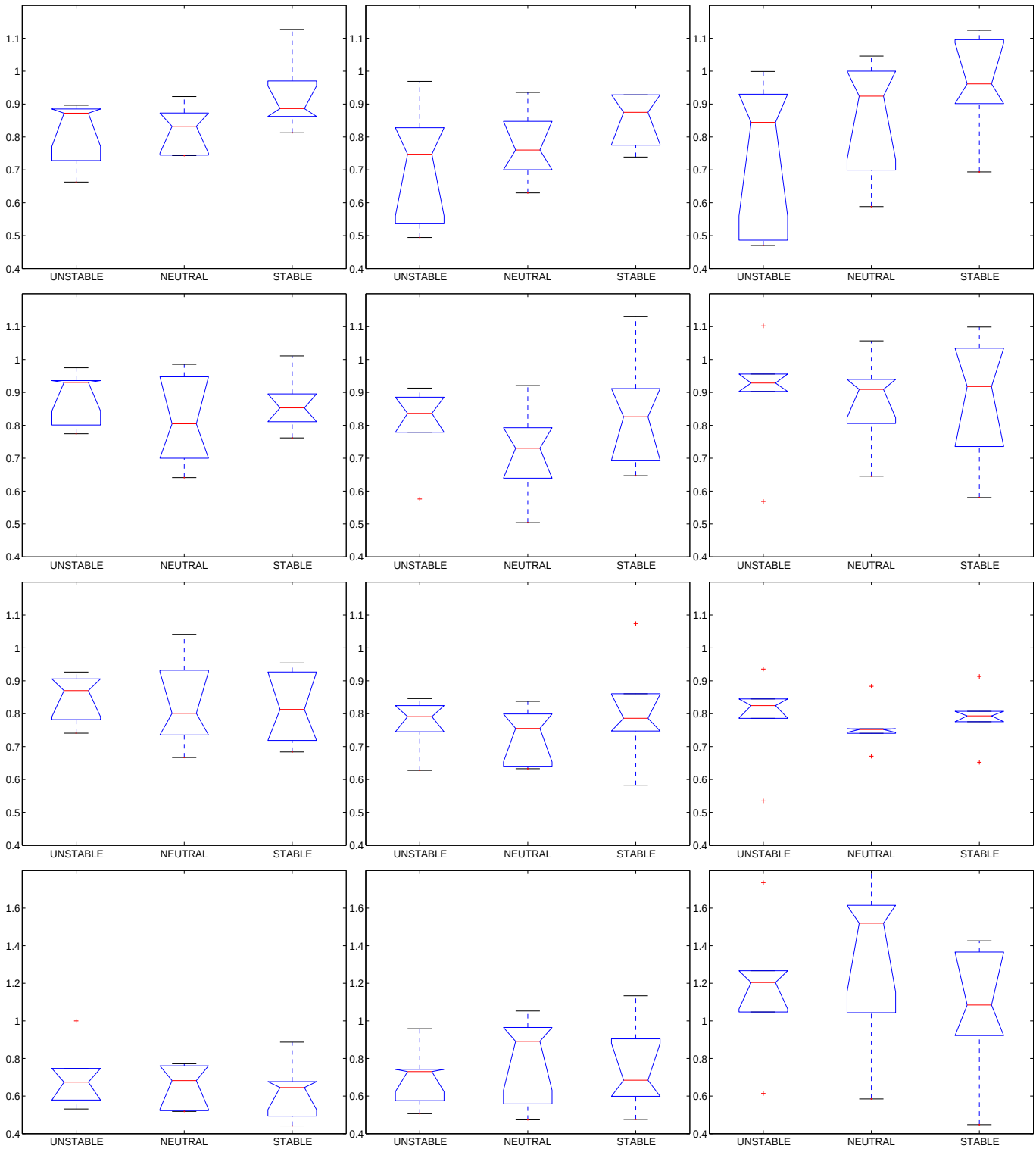

Figure 4: Box plots of the shape coefficients in $\mathcal{EPD}$ model across different stability regimes. The four rows correspond to u, v, w and T respectively from the top to the bottom. The three finest scales of wavelet coefficients are used here. The results in the left panels are from the coarsest level of wavelet decomposition while the right panels refer to the finest level.

Table 3: Mean and standard deviation of β's for all four flow variables and stability classes. Recall that $\beta = 2$ for a Gaussian process.

Turbulence		u		v		w		Temperature	
β		mean	std.	mean	std.	mean	std.	mean	std.
$j = 16$	unstable	0.8195	0.0986	0.8912	0.0824	0.8493	0.0731	0.701	0.1715
	neutral	0.8246	0.074	0.8138	0.1479	0.8296	0.1357	0.6565	0.1127
	stable	0.9241	0.1124	0.8642	0.0883	0.8183	0.1082	0.6315	0.1573
	All	0.8561	0.1031	0.8564	0.1087	0.8324	0.103	0.663	0.1433
$j = 15$	unstable	0.7204	0.1788	0.8044	0.122	0.7709	0.0804	0.7072	0.157
	neutral	0.7723	0.1094	0.7196	0.1457	0.7367	0.0845	0.8054	0.234
	stable	0.9068	0.1831	0.8394	0.173	0.8062	0.161	0.747	0.2365
	All	0.7999	0.1712	0.7878	0.1487	0.7713	0.1117	0.7532	0.2038
$j = 14$	unstable	0.7624	0.2286	0.8978	0.1768	0.7918	0.1356	1.1785	0.3625
	neutral	0.8636	0.1802	0.8776	0.1404	0.7587	0.0688	1.3546	0.4593
	stable	0.9563	0.1556	0.8808	0.1949	0.7892	0.0832	1.0551	0.3587
	All	0.8608	0.1967	0.8854	0.162	0.7799	0.0953	1.1961	0.3931

5 Discussion

To explore how atmospheric stability impacts the global scaling properties, we also show Boxplots (Figure 5) of the quasi-Hurst exponents for all the 95 turbulence measurements. Interestingly, we find that the ranges of these exponents almost coincide for the four flow variables, for which the range is between 0.28 to 0.48. In the u and v cases the ranges at different stability regimes differ, at least the stable and unstable regimes. For u and v, it is also noted that the quasi-Hurst values of measurements in the stable regime are much closer to $H = 1/3$, which is the theoretical value based on K41, than those in the other two regimes. For w and T, the ranges overlap. Another important finding is that the ranges of quasi-Hurst exponents in individual atmospheric stability regimes are much tighter for the horizontal velocity than for the other flow variables. This implies that at a fixed atmospheric stability condition, the global fractal fluctuation of the horizontal velocity is much smaller than for the other variables. Also, the horizontal velocity is characterized by greater quasi-Hurst exponents in the unstable regime than in the stable one, which means the turbulence is more "noisy" in the stable regime.

Additionally, the distributions of the quasi-Hurst exponents in the neutral regime look similar to those in the unstable, i.e., the neutral measurements tend to be similar as the unstable ones in terms of the global fractal characteristics. This is consistent for all of the four variables.

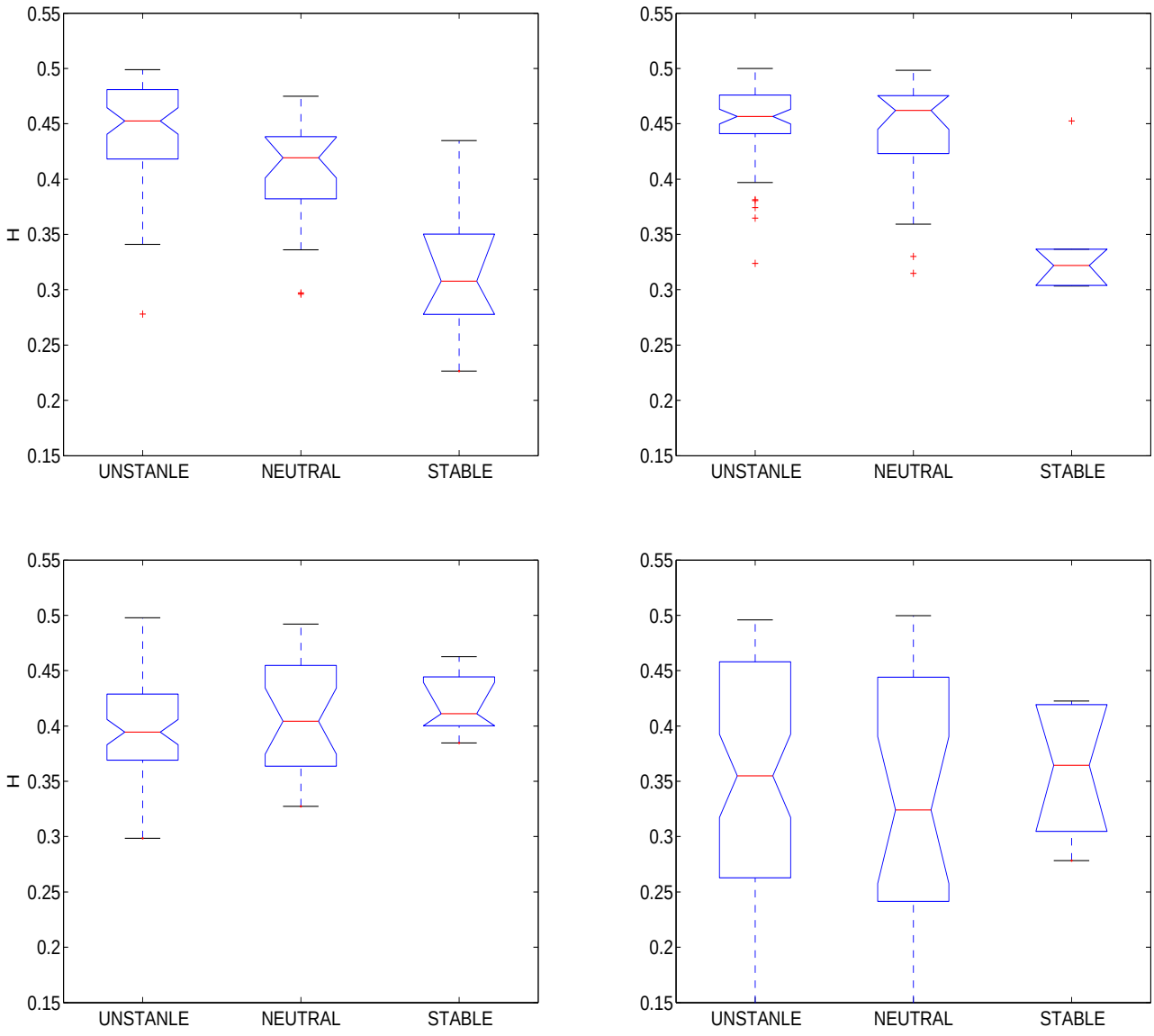

Figure 5: Box plots of the quasi-Hurst exponents $\hat{H}$ for four flow variables u, v, w, T, from the top-left to the bottom-right respectively.

The scale-wise comparison provides complementary evidence for the above arguments. The "average" pdf's (in Mallat's model) associated with atmospheric stability conditions

of the four flow variables at the three finest scales are computed. To obtain such pdf's, we averaged the estimated parameters (including both the shape parameters and scale parameters) within a stability regime and use these averages as new parameters to specify the scale-wise pdf's for each flow variable (see Figure 6). The plots in Figure 6 also suggest that u and v appear to be sensitive to atmospheric stability while w is not. However, contrary to the global analysis, the local analysis here suggests that the inertial subrange of temperature is also sensitive to atmospheric stability.

6 Conclusions

This study assessed the effects of atmospheric stability on the inertial subrange structure of u, v, w, and T using both local and global measures in the wavelet domain. The global measure relied on a quasi-hurst exponent calculation while the local measure was based on the Tsallis thermostatistic entropy approach shown to be analogous to $\mathcal{EPD}(\alpha, \beta)$ family. The analysis here demonstrated the following:

(i) The Tsallis thermostatistic entropy approach reproduces reasonably well the scale-wise velocity and temperature properties within the inertial subrange and for all stability classes, consistent with several recent studies.

(ii) The global measures were less sensitive to atmospheric stability than the scale-wise measures. In particular, the global measure identified the u and v components as the only flow variables whose inertial subrange was statistically impacted by atmospheric stability. On the other hand, atmospheric stability clearly impacted the parameters of $\mathcal{EPD}(\alpha, \beta)$ for u, v, and T flow.

(iii) The local or scale-wise analysis clearly identified dissimilarities in the intermittency between temperature and velocity even within the same stability class.

(iv) The scale-wise analysis demonstrates that the distributional properties of the velocity and temperature within the inertial subrange are far from Gaussian and with tails even heavier than a double-exponential for all stability classes.

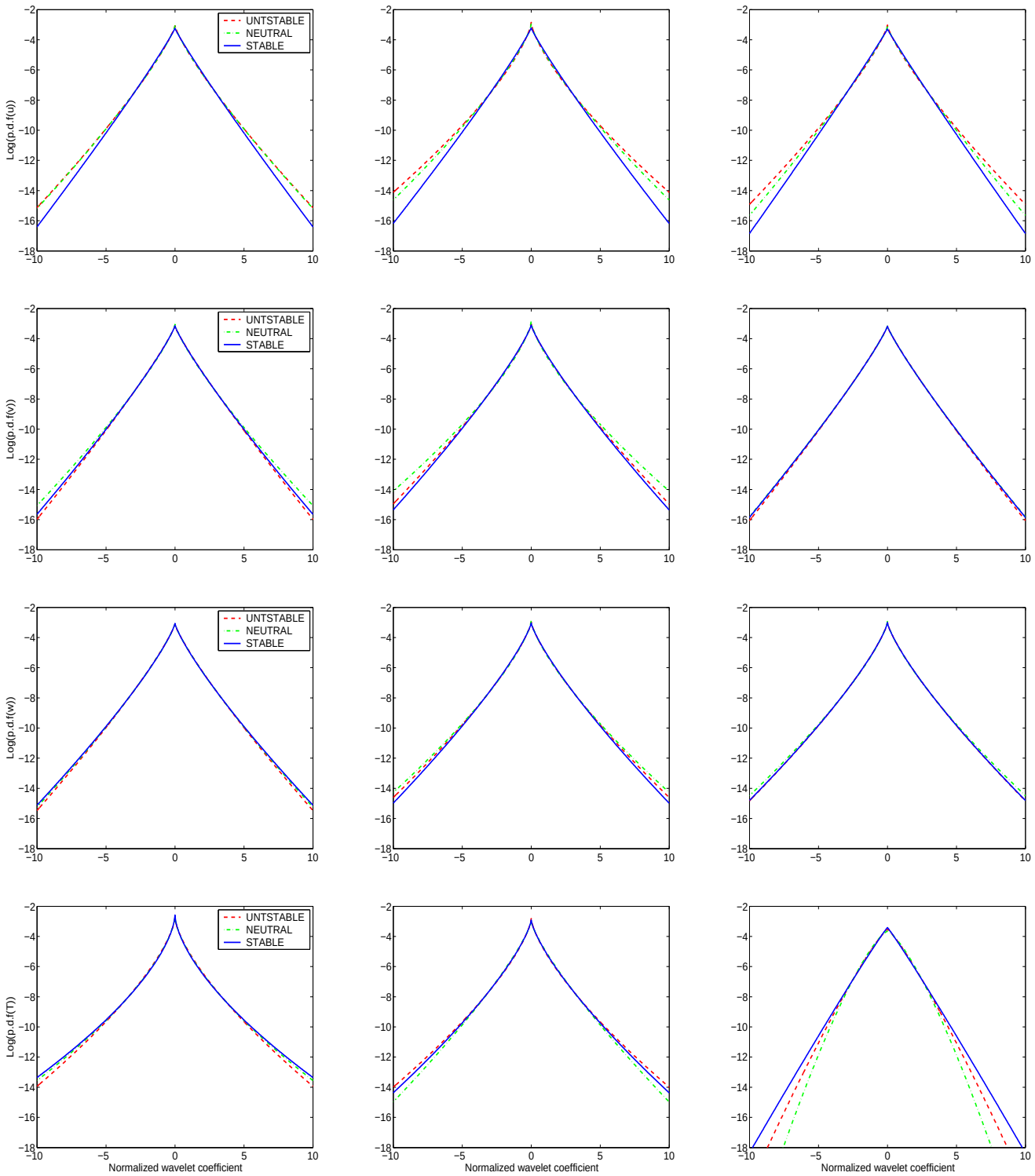

Figure 6: The average pdf's associated with stability conditions of the four flow variables (u, v, w, T) at first three finest scales. The four rows are corresponding to measurement u, v, w and T respectively from the top to the bottom. Three finest scales of wavelet coefficients are used here. The results in the left panels are from the coarsest level of wavelet coefficients while the right panels refer to the finest level.

Acknowledgments. This project was supported by the National Science Foundation (*EAR-0208258,DMS-0072585*), and *NSA-24-60R*). The experiments are part of a long-term CO2 flux monitoring initiative supported by the Office of Science (BER), U.S. Department of Energy, Cooperative Agreement No. DE-FC02-03ER63613.

Appendix: $\mathcal{EPD}$ Distribution as Tsallis MaxEnt Solution

In this Appendix we discuss a theoretical link between Tsallis Entropy and $\mathcal{EPD}(\alpha, \beta)$ family. It is demonstrated that the Maxent solution is the marginal likelihood obtained from the $\mathcal{EPD}(\alpha, \beta)$ model when the prior on β is the Inverse Gamma. In other words, the Maxent solution is the scale mixture of $\mathcal{EPD}$ distributions with the inverse gamma as mixing distribution.

Consider a random variable X distributed as the Exponential Power Family with conditional pdf given by

$$f(x|\alpha, \beta) = K \exp\left(-(|x|/\alpha)^{\beta}\right). \tag{A1}$$

Under the Bayesian paradigm, the scale parameter α is considered random and given a prior distribution. The marginal likelihood distribution of X given β is then obtained by integrating out α. Assume that $\lambda = \alpha^{-1}$ has prior distribution Gamma$(\frac{n}{2}, \frac{n}{2\lambda_0})$ with density

$$g(\lambda) = \frac{1}{\Gamma(\frac{n}{2})} \left(\frac{n}{2\lambda_0}\right)^{\frac{n}{2}} \lambda^{\frac{2}{n}-1} \exp\left\{-\frac{n\lambda}{2\lambda_0}\right\}, \tag{A2}$$

with $\lambda_0 = E(\lambda)$.

Combining (A1)and (A2) we have

$$f(x|\beta) = \int_{-\infty}^{\infty} f\left(x|1/\lambda, \beta\right) g(\lambda) d\lambda. \tag{A3}$$

There exists a closed form solution of this integral given by

$$f(x|\beta) = \frac{1}{K_q}(1 + (q-1)\lambda_1|x|^\beta)^{\frac{1}{1-q}}, \tag{A4}$$

where

$$q = 1 + \beta/(\beta n/2 + 1) \tag{A5}$$

$$\lambda_1 = \frac{\beta}{1+\beta-q}\lambda_0, \tag{A6}$$

and

$$K_q = \int_{-\infty}^{\infty}(1 + (q-1)\lambda_1|x|^\beta)^{\frac{1}{1-q}}dx. \tag{A7}$$

Hence, when the shape parameter is assumed from a particular prior, the marginal likelihood obtained from the model $\mathcal{EPD}$ in a Bayesian fashion is the Maximum Tsallis Entropy solution.

References

[1] J. Someria, "Unweaving the whirls", *Nature*, **413**, 575(2001).

[2] U. Frisch, *Turbulence*(Cambridge University Press, 296 pp., 1995).

[3] K. R. Sreenivasan, and R. A. Antonia, "The phenomenology of small scale turbulence", *Annual Reviews of Fluid Mechanics*, **29**, 435(1997).

[4] U. Frisch, A. Mazzino, and M. Vergassola, "Intermittency in passive scalar advection", *Phys. Rev. Lett*, **80** 5532(1998).

[5] B. I. Schraiman, and E. D. Siggia, "Scalar Turbulence", *Nature*, **405**, 439(2000).

[6] L. Biferale and M. Vergassola, "Isotropy vs anisotropy in small-scale turbulence", *Physics of Fluids*, **13**, 2139(2001).

[7] Z. Warhaft, "Passive scalars in turbulent flows", *Annual Reviews of Fluid Mechanics*, **32**, 203(2000)

[8] A. N. Kolmogorov, "Local structure of turbulence in an incompressible fluid for very large Reynolds numbers", *Dokl. Akad. Nauk. SSSR*, **30**, 299(1941).

[9] A. N. Kolmogorov, "A refinement of previous hypotheses concerning the local structure of turbulence in a viscous incompressible fluid at high Reynolds number", *Journal of Fluid Mechanics*, **13**, 82(1962).

[10] A. Pumir, and B. I. Shraiman, "Persistent small scale anisotropy in homogeneous shear flows", *Physical Review Letters*, **75**, 3114(1995).

[11] A. Celani, A. Lanotte, A. Mazzino, and M. Vergassola, "Universality and saturation of intermittency in passive scalar turbulence", *Phys. Rev. Lett*, **84**, 2358(2000).

[12] N.V. Antonov and J. Honkonen, "Anomalous scaling in two models of passive scalar advection: Effects of anisotropy and compressibility", *Phys. Rev. E*, **63**, 036302-1(2001).

[13] J.D Albertson, G.G. Katul, M.B. Parlange, and W.E. Eichenger, "Spectral scaling of static pressure fluctuations in the atmospheric surface layer: the interaction between large and small scales", *Physics of Fluids*, **10**, 1725(1998).

[14] A. Celani, and M. Vergassola, "Statistical geometry in scalar turbulence", *Phys. Rev. Lett*, **86**, 424(2001)

[15] G.G. Katul, C.I. Hsieh and J. Sigmon, "Energy-inertial scale interaction for temperature and velocity in the unstable surface layer", *Boundary Layer Meteorology*, **82**, 49(1997).

[16] G.G. Katul, B. Vidakovic, and J.D. Albertson, "Estimating global and local scaling exponents in turbulent flows using wavelet transformations", *Physics of Fluids*, **13**, 241(2000).

[17] H. E. Hurst, "Long-Term Storage Capacity of Reservoirs", *Proc. American Society of Civil Eng.,* **76**, 11(1950).

[18] J.F. Coeurjolly, "Simulation and identification of the fractional Brownian motion: a bibliographical and comparative study", *Journal of Statistical Software* **07**, (2000)

[19] S.G. Mallat, "A theoy for multiresolution signal decomposition: the wavelet reprentation", *IEEE Trans. on Patt. Anal. Mach. Intell.*, **11**(7), 674(1989).

[20] C. Beck, "Generalized statistical mechanics and fully developed turbulence", *Physica A*, **306**, 189(2002).

[21] M.E. Havrda and F. Charvat, "Quantification method of classification processes: Concept of structural α-entropy", *Kibernetica,* **3**, 30(1967).

[22] C. Beck, "On the small-scale statistics of Lagrangian turbulence", *Physica A*, **287**, 240(2001).

[23] T. Arimitsu and N. Arimitsu, "Analysis of fully developed turbulence in terms of Tsallis statistics", *Physical Review E*, **61**(3), 3237(2000).

[24] T. Arimitsu and N. Arimitsu, "Tsallis statistics and Turbulence", *Chaos, Solitons and Frctals*, **13**, 149(2002).

[25] T. Arimitsu and N. Arimitsu, "PDF of velocity fluctuation in turbulence by a statistics based on generalized entropy", *Physica A*, **305**, 218(2002).

[26] F.M. Ramosa, R.R. Rosaa , C.R. Netoa et al, "Non-extensive statistics and three-dimensional fully developed turbulence" *Physica A*, **295**, 250(2001).

[27] G.G. Katul, C. T. Lai, J.D. Albertson, B. Vidakovic, K. Schafer, C.I. Hsieh, R. Oren, "Quantifying the complexity in mapping energy inputs and hydrologic state variables into land-surface fluxes",*Geophysical Research Letters*, **28**, 3305(2001).

[28] C. Tsallis, "Possible generalizatopn of Boltzmann-Gibbs statistics", *J. Statist. Phys.*, **52**, 479(1988).

[29] C. Tsallis, R. S. Mendes and A. R. Plastino, "The role of constraints within generalized nonextensive statistics", *Physica A*, **261**, 534(1998).

[30] D. Prato, and C. Tsallis, "Nonextensive foundation of Levy distributions", *Phys. Rev. E*, **60**, 2398(1999)

[31] G.G. Katul, C.I. Hsieh and J. Sigmon, "Energy-inertial scale interaction for temperature and velocity in the unstable surface layer", *Boundary Layer Meteorology*, **82**, 49(1997).